ISSN No: 2348-4845
International Journal & Magazine of Engineering, Technology, Management and Research
A Peer Reviewed Open Access International Journal

A Novel Bidirectional Converter Based Space Vector Modulation Fed VSI for Electric Vehicle Applications

Kanakamedala Poojitha
M.Tech,
Department of PEED,
HITAM Engineering College.

K.Suresh
Associate Professor,
Department of EEE,
HITAM Engineering College.

Abstract:
This paper focuses on space vector modulation and core size optimization of power inductors in bidirectional dc–dc converters. The importance of the inductor design project by describing important constraints such as core size and saturation is presented. The main contribution of this paper is related to the proposed dc flux cancelation technique in the bidirectional converter. A variable inductor is used to replace the power inductor in order to decrease core size by improving the ripple content of the inductor current. Space Vector Modulation is employed as a control scheme. Simulation results validate the proposed methodology showing more than 50% reduction in magnetic material for similar current levels.

Index Terms:
Electric Vehicles (EVs), inductor, SVM, nonlinear magnetic, DC–DC power converter.

I. INTRODUCTION:

With natural resources depleting at an alarming pace and the increase of pollution, the Smart Grid has been recognized as a promising technology advancement to address these issues [1,2]. For the same reason, electric vehicles (EV) with their zero emission characteristics have become a main driving force in the automotive industry as the greener vehicles of the next generation [3,4]. While integration of large quantities of electric vehicles into the grid brings new technical and infrastructure challenges for sustained load growth and management, it also presents new opportunities in providing flexibility in power management in distribution networks [5,6]. In particular, beyond their typical roles as loads to a power system, electric vehicle battery systems can serve as distributed energy storage for grid power management. Managed properly, they can potentially improve the reliability and stability of utility grids, support integration of renewable energy generations, and improve overall system efficiency, leading to the concept of vehicle-to-grid (V2G) [7–12]. In recent years, there has been growing interest in V2G. The research on its impact on power systems has intensified recently since more and more scholars have focused on the V2G technologies. Among them, control strategies for different control objectives are the most studied topics. In [13] the authors aimed to minimizing load variance in household micro girds.

In [14,15], a two-stage optimization model is adopted to minimize the peak load and load fluctuation. V2G control strategies aiming at peak shaving and valley filling are presented in [16–19], with costs of all energy resources and system operation as the minimization objective. Bidirectional converter topologies have been studied extensively as electric vehicles chargers. They can be divided into two basic classes: off-board bidirectional chargers and on-board bidirectional chargers. Off-board bidirectional chargers commonly employ two-stage topologies that combine a three-phase pulse width modulation (PWM) converter and a bidirectional DC-DC converter.

ISSN No: 2348-4845
International Journal & Magazine of Engineering, Technology, Management and Research
A Peer Reviewed Open Access International Journal

Their components typically are of large power rating and size, and they are often used in rapid charging and discharging applications. Due to their power rating, size, cost, and noise, off-board bidirectional chargers are more suitable for commercial charging stations, rather than residential areas. The main objective of this paper is to present an adequate design of the power inductor without using interleaving techniques by proposing two approaches, i.e., initially, by an appropriate selection of core material. It is a common practice to build inductors with gapped cores to prevent saturation. Powder alloy or powder iron cores are manufactured from highly compressed powdered ferrous alloy or iron. Small air gaps are evenly distributed throughout the core material, and

This acts in a similar way to gapping a ferrite core. This allows reducing core saturation at high levels of current. The second approach proposes a variable inductor (VI) in order to decrease core size and improve the ripple content of the inductor current by controlling the saturation of the core. By actively reducing the ripple content in peak load demands, it is possible to inject more current in the same core volume or maintain the same level of current for a smaller volume core. This overall reduction in size contributes to provide more usable space for batteries and/or SCs, increasing autonomy, which is critical in today's EVs. This technique will prove its exceeding potential when aiming for more efficient EVs using an energy storage system with very high specific power.

A VI is a multiple-winding dc current-controlled device usually built with a ferrite core. As a response to the control current, the effective global reluctance of the core can be changed since the amount of dc flux in the core is varied, and therefore, differential inductance of the inductor can be controlled. Experimental results will demonstrate that a core size reduction of more than 50% can be achieved with the proposed ripple reduction technique. VIs have proven their efficacy in numerous applications with different power electronic converter topologies (i.e., ac–dc and dc–dc).

The use of variable inductances can be found in resonant converter topologies (fluorescent lamp and LED lamp drivers), power factor correction circuits, maximum power point tracking techniques, zero-voltage switching techniques, inductive power transfer systems, and also compensation schemes for ac voltage control. In addition, several papers have been recently published that deal with ripple compensation or ripple cancelation techniques using low-voltage multiple-winding inductors or integrated magnetic. Currently, no solutions have been presented yet for higher power level industrial applications with such low-level complexity implementation. This paper also focuses on the fact that small-signal inductance models do not express the behavior of power inductors under the high-current stresses expected from these systems. For simulation and design purposes, one option is to use the data provided by the manufacturer. However, it is shown that the large-signal inductance behavior can be easily obtained using sys-tem identification tools through experimental measurements of voltage and current waveforms at the power inductor terminals.

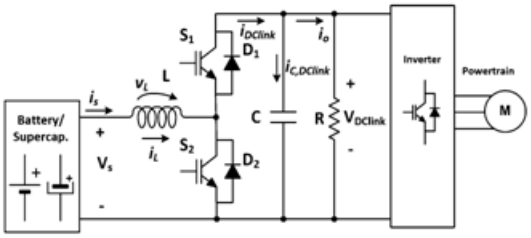

Fig. 1. Schematic of the bidirectional dc–dc converter.

II. BIDIRECTIONAL DC–DC CONVERTER AND POWER INDUCTOR:

A. Bidirectional DC–DC Converter Operation and Features:

The bidirectional dc–dc converter shown in Fig. 1 represents a reduced-scale power version, i.e., 1 kW, of the converter already introduced. The converter is a half-bridge insulated-gate bipolar transistor (IGBT) topology, or two-quadrant class-D chopper, operating in continuous conduction mode (CCM), supplied by a battery bank or by SCs.

ISSN No: 2348-4845
International Journal & Magazine of Engineering, Technology, Management and Research
A Peer Reviewed Open Access International Journal

The topology operates in boost mode for traction operation or in buck mode in cases of regenerative braking. DC-link current i_{DClink} is either positive or negative, and the voltage across the power train is always positive. In boost mode, S_2 and D_1 are active and the current flows to the dc link. In buck mode, S_1 and D_2 are active and the power flow is reversed. The power train corresponds to the three-phase inverter and motor load. Finally, resistor R stands for the remaining loads of the EV, such as light, heat, and control power supply. For the topology proposed in Fig. 1, the main challenge is to ensure stability and good transient performance as a response to disturbances.

These disturbances include the different operation modes of the power train loads, accelerating or regenerative braking, and input voltage variation (battery bank or SCs). Consequently, to cope with these uncertainties, it is necessary to endow strategies to keep the dc-link voltage within the inverter range, close to its nominal voltage value. The effects of large variations in v_{DClink}, on the inverter, and on the motor load, are, namely, torque losses, higher currents, and the presence of low-frequency harmonic distortion. All these effects lead to higher losses in the inverter and in the motor, which produce a temperature rise. These converters are also subject to high-current stress even in normal system operation, which finally requires high-flux-density magnetic materials for the filter inductor.

B. Power Inductor Considerations:

The behavior of the selected magnetic material is critical for the intended application of the power inductor or VI. Generally, it is desirable for the filter inductor to keep its inductance value in its normal operating range. Operation in the saturation region corresponds to a lower value of inductance, showing as consequence, an increased ripple and increased power losses.

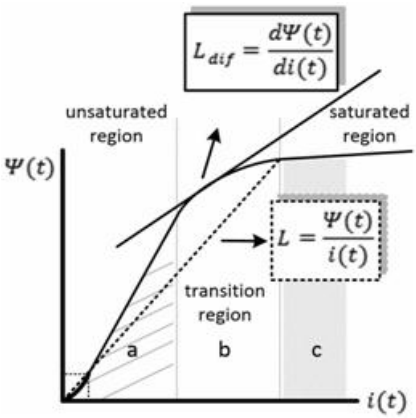

Fig. 2. Typical magnetization curve for a soft magnetic material, flux linkage as a function of current, and inductance definitions.

ferromagnetic materials, the general inductance definition is not satisfactory. In such cases, a differential inductance L_{dif} is also defined as in (1). These two definitions are graphically represented on the Ψ (t) − i(t) plane in Fig. 2.

$$L_{dif} = \frac{d\Psi(t)}{di(t)} = N\frac{d\phi(t)}{di(t)}.$$

A practical limit for the so-called linearity limit in power inductors for power converters is defined as the point where L_{dif} is reduced to half of its maximum value due to saturation effect. If the core is subject to ac and dc flux densities and the sum of these two flux densities exceeds saturation, noise, low inductance, and nonlinear effects result. For dc inductors, the standard material's choice for optimum core utilization and minimum size is to use a distributed air-gap core with a high-saturation flux density, which is the case of iron powder materials.

Permeability in the powdered cores is far less than the inherent permeability of the magnetic material used because of the many small gaps throughout the core structure. Another op-tion is to use ferrite cores. These materials have lower saturation flux density, but they have high resistivity, which keeps eddy-current losses low at higher frequencies. Soft-saturation ferrite cores will be the appointed choice for the VI implementation.

ISSN No: 2348-4845
International Journal & Magazine of Engineering, Technology, Management and Research
A Peer Reviewed Open Access International Journal

C. Estimation of the Power Inductance:

The power inductance estimation is done considering the bidirectional converter operating in both modes, buck and boost, under limit conditions for CCM operation and for a max-imum current ripple i_L of 10%. Inductor average current I_L depends on the power demands of urban driving cycles [26]. For a specific average power demand of the power train P_{Pt_avg}, the average value of the dc-link current can be calculated through (2) as follows:

$$I_{\mathrm{DClink}} = \frac{P_{\mathrm{Pt\_avg}}}{V_{\mathrm{DClink}}}.$$

I_L is calculated for the minimum value of the batteries' state of charge (SoC), which is reflected by a minimum voltage V_{bat_min} using (3) as follows:

$$L_{L\_\max} = \frac{V_{\mathrm{DClink}} I_{\mathrm{DClink}}}{V_{\mathrm{bat\_min}}}.$$

In regenerative braking, the bidirectional converter operates in buck mode. The worst condition occurs when V_{DClink} is at its maximum and the battery voltage is at its minimum value. Normal operation occurs when the battery voltage is at maxi-mum value and V_{DClink} is at nominal value. For traction mode, the bidirectional converter operates in boost mode. In this case, the worst condition occurs when V_{DClink} is at its nominal value (preferably) and the battery voltage is at its minimum value. Normal operation is the same as the buck mode. Cases where V_{DClink} is at its minimum value only occur when the supply sources are not capable of responding to the load power demand or during transient responses due to traction step loads. In this last case, the converter voltage controller will induce a higher current reference in order to restore the nominal dc-link voltage value. These transients can be neglected for the inductor design due to their occasional nature. The following sections describe the nominal inductance estimation procedure, and all necessary equations are summarized in Table I. The higher obtained inductance value will serve as reference for the power inductor prototype.

1) Buck Mode:

For buck-mode operation, with $v_s = V_{bat}$, the inductance value is calculated using (4) as follows:

$$L_{\mathrm{bat}} = \frac{V_{\mathrm{bat}}(1-D)}{\Delta i_L f_s}.$$

The duty ratio will vary between D_{min} and D_{max}. D_{max} is calculated for V_{DClink} and not V_{DClink_min}. The implemented converter control regulates the dc-link voltage level in order to keep it within appropriated values. Using the calculated value for D_{min}, L_{bat} can be obtained from (4) for the previously defined current ripple were used, a smaller.

TABLE II: POWER SETUP RATINGS

Parameters	Max [V]	Nominal [V]	Min [V]
V_{DClink}:	145	108	80
V_{bat}: (3 Ni-MH batteries from SAFT, 12 V/13 Ah)	43.5	36	28.6
V_{sc}: (18 SCs from NessCap, 100 F, 2.7 V/21.4 A)	48.6	-	24.3
Inductor current*	I_{L_avg} = 10A	$I_{L\_ac\_rms} = \sqrt{\left(\frac{1}{6}\Delta i_L\right)^2}$	$I_{L\_rms} = \sqrt{I_L^2 + \left(\frac{1}{6}\Delta i_L\right)^2}$
L_{sc_max} = 1.336 mH	C = 10mF	R = 200Ω	f_s = 20kHz

*Considering a triangular waveform with DC average value.

Inductance value would be obtained. With $v_s = V_{sc}$, the whole process is repeated for the same current ripple i_L.

2) Boost Mode:

In boost mode, the input–output voltage ratio is defined as follows:

$$V_{\mathrm{DClink}} = \frac{V_{\mathrm{bat}}}{1-D}.$$

In this case, L_{bat} is calculated using (6). L_{bat_max} and L_{bat_min} should be considered

$$L_{\mathrm{bat}} = \frac{V_{\mathrm{bat}} D}{\Delta i_L f_s}.$$

It is noted that, in boost mode, the battery current i_{bat} is equal to the inductor current. For $v_s = V_{sc}$, the process is repeated. In this case, the duty ratios and the inductance values can be calculated by using the correspondent equations presented in Table I.

ISSN No: 2348-4845
International Journal & Magazine of Engineering, Technology, Management and Research
A Peer Reviewed Open Access International Journal

Based on the obtained results, the maximum value of the power inductance was selected as the reference value for the power inductor prototype. The main goal is to ensure that the current ripple I_L is a small fraction of the full-load inductor dc component.

D. Powdered Iron Core Inductor Design:

The experimental bidirectional converter is a reduced-scale prototype for which certain specifications regarding nominal voltages are adopted: Nominal voltage for the battery bank is V_{bat} = 36 V, and for the SCs, it is V_{sc} = 48.6 V. However, the battery bank can deliver a supply voltage between 28.6 and 43.5 V, depending on the batteries' SoC, and the SCs between 48.6 and 24.3 V, which corresponds to their most efficient operating range [30]. Converter switching frequency f_s is set at 20 kHz. The dc-link nominal voltage is set at V_{DClink} = 108 V.

Typically, in commercial inverters, the rise of the dc-link voltage, when regenerative braking occurs, may be up to 30%. In normal operation, the inverter admits a lower voltage supply, about −25%, for 60 s. Considering a P_{Pt_avg} around 280 W, using (2) and (3), the average inductor current is IL avg ˜ _ = 10 A.

Following the procedure for inductance estimation, the maximum obtained value is L_{SC_max} = 1.336 mH. Table II collects all the parameters described above. L_{L,ac_rms} corre-sponds to the ac RMS value of the inductor current, and I_{L_rms} corresponds to the RMS value of the inductor current.

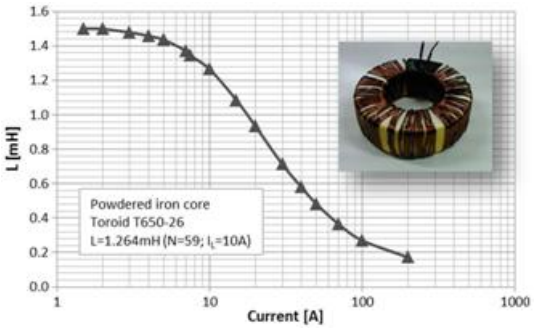

Fig. 3. Inductance curve provided by Micrometals software and induc-tor prototype.

The design of the power inductor takes into consideration a powdered iron core from Micrometals. Using the manufacturer software [31] and establishing the nominal voltages, maximum current ripple and reference inductance value for the desired power inductor, the software presents a solution. It also pro-vides the resulting inductance as a function of the inductor current, as well as the inductance as a function of temperature. Table III presents the estimated power inductor characteristics.Fig. 3 presents the inductance saturation curve as a function of the inductor current and the power inductor prototype. Rather than designing the inductor for the average selected value of 10 A, the maximum required inductor current occurring during the higher power demand stresses, approximately 35 A, is considered. Completely avoiding core saturation and therefore operating in the constant part of the L(i) curve would imply a nonacceptable increase in core size and volume [26]. The small-signal inductance value of the power inductor was experimen-tally obtained with an LCR meter, giving L =1.557 mH at 1 A.

III. SPACE VECTOR MODULATION SCHEME:

Space vector modulation (SVM) is an algorithm for the control of pulse width modulation (PWM). It is used for the creation of alternating current (AC) waveforms; most commonly to drive 3 phase AC powered motors at varying speeds from DC using multiple class-D amplifiers. There are variations of SVM that result in different quality and computational requirements. One active area of development is in the reduction of total harmonic distortion (THD) created by the rapid switching inherent to these algorithms. A three-phase inverter as shown to the right converts a DC supply, via a series of switches, to three output legs which could be connected to a three-phase motor. The switches must be controlled so that at no time are both switches in the same leg turned on or else the DC supply would be shorted. This requirement may be met by the complementary operation of the switches within a leg. i.e. if A^+ is on then A^- is off and vice versa.

ISSN No: 2348-4845
International Journal & Magazine of Engineering, Technology, Management and Research
A Peer Reviewed Open Access International Journal

This leads to eight possible switching vectors for the inverter, V_0 through V_7 with six active switching vectors and two zero vectors.

Vector	A⁺	B⁺	C⁺	A⁻	B⁻	C⁻	V_{AB}	V_{BC}	V_{CA}	
V_0 = (000)	OFF	OFF	OFF	ON	ON	ON	0	0	0	zero vector
V_1 = (100)	ON	OFF	OFF	OFF	ON	ON	$+V_{dc}$	0	$-V_{dc}$	active vector
V_2 = (110)	ON	ON	OFF	OFF	OFF	ON	0	$+V_{dc}$	$-V_{dc}$	active vector
V_3 = (010)	OFF	ON	OFF	ON	OFF	ON	$-V_{dc}$	$+V_{dc}$	0	active vector
V_4 = (011)	OFF	ON	ON	ON	OFF	OFF	$-V_{dc}$	0	$+V_{dc}$	active vector
V_5 = (001)	OFF	OFF	ON	ON	ON	OFF	0	$-V_{dc}$	$+V_{dc}$	active vector
V_6 = (101)	ON	OFF	ON	OFF	ON	OFF	$+V_{dc}$	$-V_{dc}$	0	active vector
V_7 = (111)	ON	ON	ON	OFF	OFF	OFF	0	0	0	zero vector

To implement space vector modulation, a reference signal V_{ref} is sampled with a frequency f_s ($T_s = 1/f_s$). The reference signal may be generated from three separate phase references using the transform. The reference vector is then synthesized using a combination of the two adjacent active switching vectors and one or both of the zero vectors. Various strategies of selecting the order of the vectors and which zero vector(s) to use exist. Strategy selection will affect the harmonic content and the switching losses.

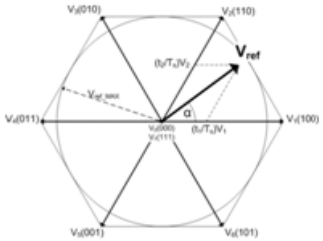

IV. SIMULATION RESULTS:

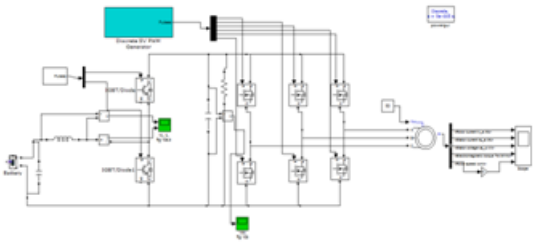

Fig. 8. Bidirectional dc–dc converter:

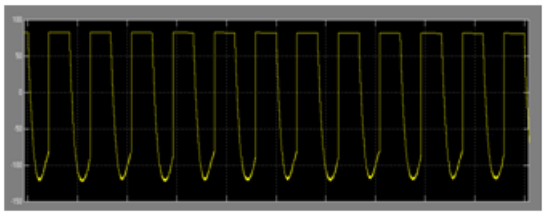

Fig. 9. Buck-boost mode operation. Power inductor operating

buck mode, it was possible to reach a higher value for the inductor current, around 40 A. Examples of the experimental waveforms, for buck and boost modes, are respectively pre-sented in Figs. 9(a) and 10(a). It is possible to observe the inductor voltage and current, as well as the dc-link voltage for duty cycles D = 74% and D = 67.5%, respectively. Figs. 9(b) and 10(b) both show the

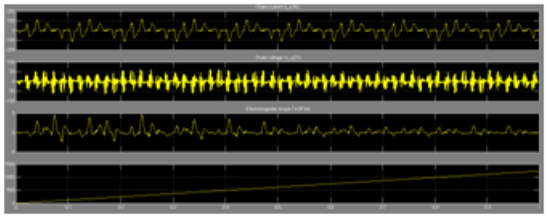

Fig. 10. Buck-Boost-mode operation: stator current, stator voltage, torque & speed

Experimental inductor current waveform for a higher level of I_L. For higher current values, in both operation modes, a noise problem was observed during IGBT switching. Current spikes were suppressed when using the system identification toolbox. Large-signal characterization was done considering initial guess values for the constant set at $k = 20\ \Omega^{-1}$ and $\tau = 0.0245$ s. The inductance curves as function of the average inductor current $L(I_L)$ for both operation modes are shown in Fig. 11. These two curves correspond to the processed data for both operating modes, traction, and regenerative braking. Theoretically, these curves should coincide; however, in boost and buck modes, for the same current level, the current ripple is slightly different, and therefore, a different value of the inductance should be expected. In addition, obtaining the experimental data for exactly the same conditions is difficult since terminal voltage of batteries and SCs increases or decreases during the operation range.

ISSN No: 2348-4845
International Journal & Magazine of Engineering, Technology, Management and Research
A Peer Reviewed Open Access International Journal

Fig. 11 also shows the Micrometals software curve for comparison. If the manufacturer curve is obtained as a function of a dc current without ripple, this difference is justi-fied. In addition, large-signal characterization curves will show higher inductance values. Saturation of the power inductor in the high current range is clearly observed. Corresponding fitting curves are also presented.

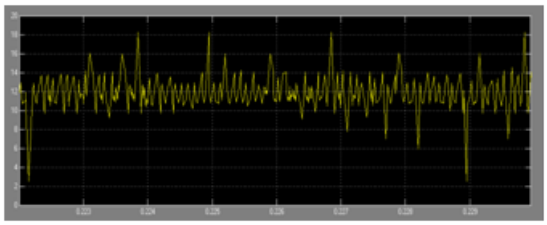

Fig. 11. Large-signal inductance curve for buck mode and boost mode, i.e., $L(I_L)$.

V. CONCLUSION:

A power inductor was designed for a reduced-scale 1-kW bidirectional converter prototype. The design method was based on a core size optimization approach, and a powdered iron core material was selected because of the good behavior of such materials under high-current-stress conditions. This paper provides a solution for core size optimization of the power inductor through a current ripple reduction technique. The proposed technique solves a critical issue regarding the saturation of power inductors during the request of high amounts of energy for hard acceleration and braking operations. Inductors with extra auxiliary windings recently have been used to increase the transient performance of dc–dc converters are presented by the Matlab Simulation.

REFERENCES:

1. Amin, S.M.; Wollenberg, B.F. Toward a smart grid: Power delivery for the 21st century. IEEE Power Energy Mag. 2005, 3, 34–41.

2. Ipakchi, A.; Albuyeh, F. Grid of the future. IEEE Power Energy Mag. 2009, 7, 52–62.

3. Chan, C.C. The state of the art of electric and hybrid vehicles. Proc. IEEE 2002, 90, 247–275.

4. Chan, C.C. The state of the art of electric, hybrid, and fuel cell vehicles. Proc. IEEE 2007, 95, 704–718.

5. Clement-Nyns, K.; Haesen, E.; Driesen, J. The impact of charging plug-in hybrid electric vehicles on a residential distribution grid. IEEE Trans. Power Syst. 2010, 25, 371–380.

6. Lopes, J.A.P.; Soares, F.J.; Almeida, P.M.R. Integration of electric vehicles in the electric power system. Proc. IEEE 2011, 99, 168–183.

7. Kempton, W.; Letendre, S.E. Electric vehicles as a new power source for electric utilities. Transp. Res. Part D 1997, 2, 157–175.

8. Kempton, W.; Tomić, J. Vehicle-to-grid power fundamentals: Calculating capacity and net revenue. J. Power Sources 2005, 144, 268–279. Energies 2014, 7 4890

9. Kempton, W.; Tomić, J. Vehicle-to-grid power implementation: From stabilizing the grid to supporting large-scale renewable energy. J. Power Sources 2005, 144, 280–294.

10. Tomić, J.; Kempton, W. Using fleets of electric-drive vehicles for grid support. J. Power Sources 2007, 168, 459–468.

11. Clement-Nyns, K.; Haesen, E.; Driesen, J. The impact of vehicle-to-grid on the distribution grid. Electric Power Syst. Res. 2011, 81, 185–192.

12. Yu, Y.F.; Zhang, Q.F.; Liang, B.; Liu, X.F.; Cui, S.M. Analysis of a single-phase Z-source inverter for battery discharging in vehicle to grid applications. Energies 2011, 4, 2224–2235.

13. Jian, L.N.; Xue, H.H.; Xu, G.Q.; Zhu, X.Y.; Zhao, D.F.; Shao, Z.Y. Regulated charging of plug-in hybrid electric vehicles for minimizing load variance in household smart microgrid. IEEE Trans. Ind. Electron. 2013, 60, 3218–3226.

14. Luo, Z.W.; Hu, Z.C.; Song, Y.H.; Xu, Z.W.; Lu, H.Y. Optimal coordination of plug-in electric vehicles in power grids with cost-benefit analysis—Part I: Enabling techniques. IEEE Trans. Power Syst. 2013, 28, 3546–3555.

15. Luo, Z.W.; Hu, Z.C.; Song, Y.H.; Xu, Z.W.; Lu, H.Y. Optimal coordination of plug-in electric vehicles in power grids with cost-benefit analysis—Part II: A case study in China. IEEE Trans. Power Syst. 2013, 28, 3556–3565.

16. Wang, Z.P.; Wang, S. Grid power peak shaving and valley filling using vehicle-to-grid systems. IEEE Trans. Power Deliver. 2013, 28, 1822–1829.

17. Soares, J.; Morais, H.; Sousa, T.; Vale, Z.; Faria, P. Day-ahead resource scheduling including demand response for electric vehicles. IEEE Trans. Smart Grid 2013, 4, 596–605.

18. Yao, W.F.; Zhao, J.H.; Wen, F.S.; Xue, Y.S.; Ledwich, G. A hierarchical decomposition approach for coordinated dispatch of plug-in electric vehicles. IEEE Trans. Power Syst. 2013, 28, 2678–2778.

19. Mu, Y.F.; Wu, J.Z.; Ekanayake, J.; Jenkins, N.; Jia, H.J. Primary frequency response from electric vehicles in the great britain power system. IEEE Trans. Smart Grid 2013, 4, 1142–1150.

20. Geng, B.; Mills, J.K.; Sun, D. Two-stage charging strategy for plug-in electric vehicles at the residential transformer level. IEEE Trans. Smart Grid 2013, 4, 1442–1452.

Author Details

Kanakamedala Poojitha, Received B.Tech degree fromTRR Engineering college for womens, Inole (V), Patancheru (M), Medak(D), Telangana in 2013. And currently pursuing M.Tech in Power electronics & electrical drives at Hyderabad institute of technology and management, Gowdavelly, Medchalmandal, R.R.district, Telangana. Her area of interest in Power Electronics field.

K.Suresh, Obtained his B.Tech (EEE) degree from shadhan group of engineering Technology, Peerancheru, HimayathSagar Road, JNTUH in 2004, M.Tech (Power Electronics) from JNTUH in 2011. He has been working as Associate Professor in dept. of EEE at HITAM Hyderabad since 2008. His area of interest include power electronics & electrical circuits. He is having 10 years of teaching experience.